Chemosphere 268 (2021) 129266

Contents lists available at ScienceDirect

Chemosphere

journal homepage: www.elsevier.com/locate/chemosphere

Investigating the impact of *in situ* soil organic matter degradation through porewater spectroscopic analyses on marsh edge erosion

Michael P. Hayes [a, 1], Yadav Sapkota [b, 1], John R. White [b, *], Robert L. Cook [a, **]

[a] Department of Chemistry, Louisiana State University, Baton Rouge, LA, USA
[b] Wetland and Aquatic Biogeochemistry Laboratory, Department of Oceanography & Coastal Sciences, Louisiana State University, Baton Rouge, LA, USA

HIGHLIGHTS

- Significant edge erosion is occurring at relatively "protected" islands.
- *In situ* soil organic matter degradation did not well correlate to marsh edge erosion.
- Drivers of edge erosion are complex including waves, soil properties, and organic matter degradation.
- The eroded wetland soil organic matter is not reburied in the estuarine bottom.

ARTICLE INFO

Article history:
Received 27 October 2020
Received in revised form
8 December 2020
Accepted 8 December 2020
Available online 10 December 2020

Handling Editor: Willie Peijnenburg

Keywords:
Sea-level rise
Blue carbon
Coastal erosion
Climate change
CO_2 emission
Ultraviolet–Visible (UV–Vis)
Fluorescence

ABSTRACT

Marsh edge erosion results in soil organic matter (SOM) loss from coastal wetlands and is differentially affected by wind waves, soil properties, and vegetation cover. The degradation of SOM may make the marsh edge susceptible to erosion. The objective of this study was to investigate the effect of *in situ* biogeochemical degradations of SOM on marsh edge erosion using porewater spectroscopic analyses. Edge erosion was monitored at 12 transects in one of the highly eroding coastal basins of Louisiana. A total of 36 cores were collected at different distances from the edge of the marsh. Porewater was extracted and analyzed for dissolved organic carbon (DOC) and spectroscopic indicators. The north and west side had greater erosion rates (102.38 ± 5.2 cm yr^{-1}) than east and south side (78.47 ± 3.3 cm yr^{-1}). However, the north and east side had greater DOC and refractory carbon but less microbial activity indicating SOM degradation alone did not correlate to edge erosion. The intersecting trend between erosion rate and SOM degradation among four sides of the island indicates the complex nature of edge erosion drivers. The estuarine bottom indicators suggest the eroded SOM is not reburied but rather degraded and emitted back into the atmosphere as CO_2, potentially contributing to global change. The coastlines projected to experience high sea-level rise in the coming century are vulnerable to losing a large amount of stored carbon in the absence of efficient mitigation measures.

1. Introduction

Wetlands store approximately one-third of the world's soil carbon, estimated at 530 Pg C, but only encompasses 5–6% of the world's land surface (Reddy and DeLaune, 2008). Maintaining these soil carbon pools is vital to regulating the global carbon cycling as well as nutrient storage and dispersal (Whiting and Chanton, 2001; Bridgham et al., 2006). The amount of carbon stored in wetland soils is roughly equivalent to 75% of the atmospheric carbon pool, making this small land surface disproportionately critical to global carbon cycling (Choi and Wang, 2004; Williams et al., 2009).

The organic carbon accumulation in coastal wetlands can take place over long periods creating centuries worth of carbon-rich soil in the vertical depth profile. Coastal wetlands exhibit optimal conditions for both primary production and preservation of carbon (Mcleod et al., 2011). Overall, tidal, salt marshes sequester an annual average of 210 g C m^{-2} yr^{-1}, though this rate is dependent upon environmental conditions (Chmura et al., 2003). The soils

* Corresponding author. 3239 Energy, Coast and Environment Building, Department of Oceanography & Coastal Sciences, Louisiana State University, Baton Rouge, 70803, USA.
** Corresponding author. 307 Choppin Hall, Department of Chemistry, Louisiana State University, Baton Rouge, 70803, USA.
E-mail addresses: jrwhite@lsu.edu (J.R. White), rlcook@lsu.edu (R.L. Cook).
[1] Contributed Equally.

https://doi.org/10.1016/j.chemosphere.2020.129266
0045-6535/

have a variety of labile carbon compounds that are utilized by microbial communities through enzymatic degradation (Reddy and DeLaune, 2008; Fichot et al., 2012; Joshi et al., 2020). The refractory pool of carbon is more resistant to microbial degradation than the labile pool as it requires more energy to degrade. Under anaerobic conditions, microbes are unable to acquire sufficient energy to breakdown this refractory carbon pool and contributes to the long-term storage of carbon in wetland soils (Reddy and DeLaune, 2008).

Environmental conditions regulating carbon accumulation including sea-level rise, subsidence, tidal range, and episodic severe weather events, such as hurricanes, change the landscape of coastal wetlands (Chambers et al., 2019; DeLaune and White, 2012). The relatively slow sea-level rise over the last 4000 years has optimized the conditions for carbon sequestration and accumulation in wetland dominated coastlines. However, more recently, local subsidence coupled with the global sea-level rise has led to the marsh fragmentation, ponding, submergence, and edge erosion affecting the stability of wetland soil carbon stocks (DeLaune et al., 1994; DeLaune and White, 2012; Mariotti 2016; Sapkota and White, 2019). Coastal Louisiana is influenced not only by global eustatic sea-level rise but also subsidence, leading to a combined 12+ mm yr^{-1} relative sea-level rise rate (Jankowski et al., 2017). The Louisiana coastal zone contains approximately 40% of the total coastal wetlands in the contiguous United States but experiences almost 80% of the total coastal wetland land loss (Couvillion et al., 2017). The high relative sea-level rise rate may promote the accumulation of carbon in the wetlands (Schuerch et al., 2018; Rogers et al., 2019; Breithaupt et al., 2020), however, the flooding stress to plants and reduced sediment from tributaries on the Mississippi River may limit carbon accumulation (Blum and Roberts, 2009).

Numerous research studies have explored edge erosion as the primary cause of land loss and associated carbon loss from coastal wetlands (Nyman et al., 1994; Wilson and Allison, 2008; Morton et al., 2009). Studies have also identified wind waves as a primary factor (Wolters et al., 2005; McLoughlin et al., 2015; Wang et al., 2017) whereas soil physiochemical properties and vegetation cover as secondary factors of marsh edge erosion (Feagin et al., 2009; Morton et al., 2009; McLoughlin et al., 2015; Wang et al., 2017). Some studies have concluded that the marsh edge erosion rate is directly proportional to the power of the incident wave (Marini et al., 2011; Leonardi et al., 2016). The power of the incident wave is strongly related to the fetch of the water body, tidal height, and wind speed, duration, and direction (Kirby, 2000; Wilson and Allision, 2008; Valentine and Mariotti, 2019; Sapkota and White, 2019). During edge erosion, approximately the top 40 cm of peat soil at the edge of the marsh collapses due to undercutting by waves followed by submergence (Wilson and Allison, 2008; Valentine and Mariotti, 2019; Sapkota and White, 2019). The wave activity continuously dislodges submerged peat material until the bottom of the estuary achieves an equilibrium bathymetric profile (Wilson and Allison, 2008; Sapkota and White, 2019). The physical disarticulation of the eroded SOM occurs in the estuarine water and undergoes mineralization (Li et al., 2011; Steinmuller et al., 2019; Haywood et al., 2020; Sapkota and White, 2021). While most of the studies on marsh edge erosion are focused on wind waves, few studies have looked into the soil physiochemical properties including bulk density and organic matter content relative to the degree of resistance to the edge erosion (Wang et al., 2017; Valentine and Mariotti, 2019; Sapkota and White, 2019). However, the weakening of the marsh platform by *in situ* biogeochemical degradations of soil organic matter (SOM) may accelerate marsh edge erosion.

The *in situ* degradations of SOM can be assessed by porewater spectroscopic analyses including ultraviolet–visible (UV–Vis) and fluorescence (Wang et al., 2013; Clark et al., 2014; Haywood et al., 2020). These spectroscopic analyses provide information on the carbon moieties present and relative degradation in porewater and infer to the corresponding wetland soil (Cook et al., 2009; Traversa et al., 2014; Watanabe et al., 2012; Haywood et al., 2020) (Table 1). The goal of this study was to understand the role of *in situ* biogeochemical degradations of SOM on marsh edge erosion in a highly eroding coastal basin in Louisiana. This goal has been achieved by monitoring marsh edge erosion and investigating *in situ* biogeochemical degradations of SOM through a combination of geophysical and spectroscopic techniques. We hypothesize that *in situ* SOM degradation increases the marsh edge erosion rate. As

Table 1
Soil porewater spectroscopic variables measured including chemical meaning and ecological indication. Adapted and modified from Steinmuller et al. (2020) and Haywood et al. (2020).

Indicator	Measurement	Chemical Meaning	Ecological Indication	Reference
UV–Visible Indicators				
Spectral slope (S_{275})	Linear fit of Napierian absorption coefficient spectrum from 275 to 295 nm	Indicator of lignin molecular weight	Indicator of degree of degradation of DOM	Fichot and Benner (2012)
Specific UV absorbance at 254 nm ($SUVA_{254}$)	Divide absorbance at wavelength of 254 nm by DOC concentration	Concentration of aromatic carbon within porewater	Indicator of humic fraction of DOC	Weishaar et al. (2003)
$SUVA_{350}$	Divide absorbance at wavelength of 350 nm by DOC concentration	Concentration of lignin-like carbon within porewater	Indicator of fraction of larger MW compounds	Weishaar et al. (2003)
Spectroscopic Indices				
Fluorescence index (FI)	Dividing Em. intensity at 450 nm (biological) by that at 500 nm (terrestrial) with 370 nm Ex.	Autochthonous vs. allochthonous production of DOM	Degree of terrestrial nature of DOM	McKnight et al. (2001)
Biological index (BIX)	Dividing Em. intensity at 380 nm (protein) by that at 430 nm (biological) with 310 nm Ex.	Fresh protein inputs within DOM pool	Assessment of 'freshness' of biological activity within DOM pool	Huguet et al. (2009)
Humification index (HIX)	Sum of Iem 435–480 divided by sum Iem 300–345 pulse sum of Iem 435–480 at Ex. 254 nm	Red shifting of fluorophores	Extent of humification of DOM	Ohno (2002)

coastal Louisiana is currently experiencing high relative sea-level rise to the extent other coastlines in the world are projected to experience in the next 50–75 years, this study can be taken as a proxy for the future risk of the loss of soil carbon pool in wetland-dominated coastlines worldwide.

2. Materials and methods

2.1. Study area and erosion measurement

The study was conducted at a relatively "protected" island (29.466887, −89.910751) located in south Wilkinson Bay in the northeast portion of Barataria Bay, Louisiana (Fig. 1). The area of the island is approximately 0.11 km^2. Barataria Basin experiences one of the highest marsh erosion rates in the continental USA. The separation of the basin from the Mississippi River via levees has limited sediment supply over the past century. The high relative sea-level rise coupled with wind waves and limited sediment supply has resulted in a rapid land loss of approximately 13.3 km^2 y^{-1} (Couvillion et al., 2017), primarily through marsh edge erosion. The salinity of the northern bay marshes ranges from 10 to 25 practical salinity units (White et al., 2018). The dominant vegetation is *Spartina patens and Spartina alterniflora*. Barataria Bay represents a micro-tidal system with a diurnal tidal regime (Georgiou et al., 2005). The study site has four distinct facing shoreline directions (sides): north, east, south, and west (Fig. 1). The island is generally "protected" from the direct wave climate of the bay due to the presence of several large wetland tracts, however, it still experiences variable small wind wave-induced erosion on all sides (Sapkota and White, 2019).

At each of the four sides (cardinal directions), three replicate transects were established for erosion measurements in April 2018. Each erosion measurement transect consists of three PVC poles installed at the interval of 1 m starting from 1 m from the edge of the marsh. The distance from the edge of the marsh to the nearest pole was recorded at least once every three months for almost 3 years. As the erosion removes the bayward pole, a new pole was added at the inland edge of the transect. The erosion rate was calculated from the shoreline recessions over time. The estuarine depth relative to the marsh surface was measured using a metered pole at 0.2 m and 16 m offshore to construct a bathymetric profile.

2.2. Soil and water sample collection

Soil samples were collected from each of the 12 transects on four sides of the island between September and November 2018. At each transect, samples were collected from 2 m inland from the edge (−2.0 m), at the edge (+0.2 m), and within the bay (+16 m) (Fig. 1). The cores were collected utilizing an acrylic tube (1.7 m long x 7.6 cm diameter) by a manual push-coring method. The core length ranged from 0.5 m–1.0 m long with minimal compaction. The cores were extruded and sectioned into 10 cm sections in the field, sealed in polyethylene bags, and stored on ice for transportation to the lab after which they were then stored in the dark at 4 °C until processing. Surface water samples were collected from the marsh edge (+0.2 m) and in the bay (+16.0 m) along the 12 transects, 10 cm below the water surface following Haywood et al. (2018).

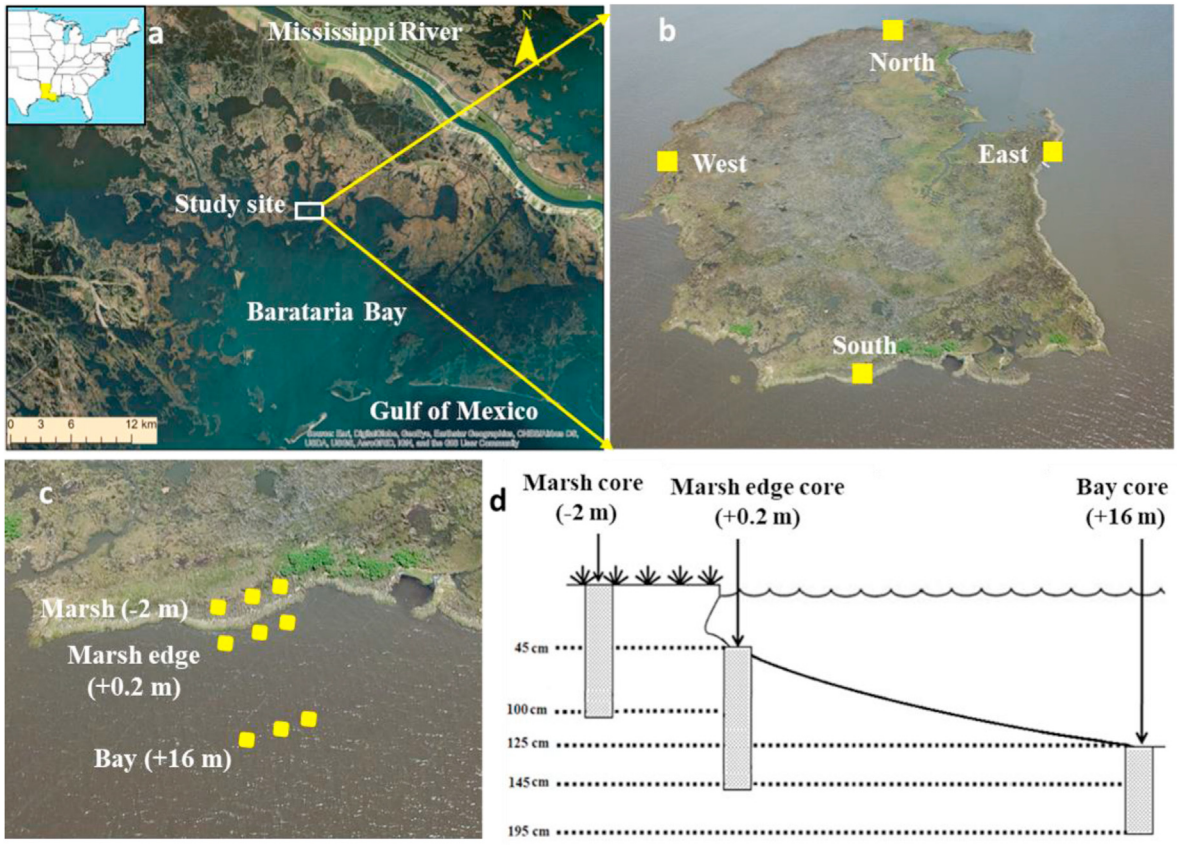

Fig. 1. Study site. a) Location of Louisiana in USA and location of study site in northern part of Barataria bay, b) Drone image of study island showing four different sides, c) Sampling transects at a side, and d) Cross-section diagram of a transect showing the depth of sampling points relative to the marsh surface.

2.3. Soil physiochemical properties analysis

At the lab, each 10 cm soil sample was weighed, homogenized, and then sub-sampled for soil physiochemical properties analyses including bulk density, moisture content, percent organic matter (% OM), and total carbon (TC). Briefly, the ~30 g field moist sub-sample was oven-dried at 60 °C until a constant weight was achieved to determine gravimetric moisture content. The bulk density of each sample was determined by calculating the total dry weight of the sample and then dividing by the volume of the 10 cm section of the core (385 cm^3). The dry sub-sample was then ground using a mortar and pestle. One gram of the dried, ground material underwent wt % OM determination by combusting in a Thermolyne furnace at 550 °C for 4 h (ThermoFischer Scientific, Waltham, MA). A subset (n = 60) of separate 8 mg sub-samples were used to determine TC by combustion at 900 °C for 13 min, via a Shimadzu Total Organic Carbon Analyzer with SSM-5000 A (Shimadzu, Columbia, MD). The relationship between TC and % OM was established by a simple linear regression model ($y = 0.45x - 0.37$; $r^2 = 0.97$), which was then used to determine TC concentrations of remaining samples.

2.4. Porewater analysis

The remaining field moist sample was centrifuged at 2578 *g* for 10 min to separate pore water from the solids. The pore water was decanted, filtered through a 0.45 μm × 25 mm Nylon syringe filter, and stored at 4 °C in the dark until analysis. The porewater was analyzed for dissolved organic carbon (DOC) using a Total Organic Carbon Analyzer (TOC-L) (Shimadzu, Columbia, MD). In addition, a Cary 100 Spectrophotometer (Varian Inc., Palo Alto, CA) was used to collect UV–Vis absorbance spectra, and a Spex Fluorolog-3 spectrofluorometer (HORIBA Scientific, Edison, NJ) was used to collect fluorescence, following Haywood et al. (2018). These UV–Vis and fluorescence data were used to derive a range of commonly used DOC spectroscopic indicators (Table 1) (Bianchi et al., 2011; Kolic et al., 2014; Haywood et al., 2018; Derrien et al., 2020). Similarly, estuarine water also underwent both DOC and spectroscopic analyses.

2.5. Statistical analysis

The analysis of variance (ANOVA) was performed on R (Version 3.5.3; R Foundation for Statistical Computing, Vienna, Austria). An ANOVA was run on all the soil physiochemical and porewater spectroscopic indicators with side, depth, and distance as fixed effects**.** The multiple comparisons were done using the Tukey HSD method and Bonferonni correction was applied to the significance level (alpha value = 0.003). The plots were prepared as means (±standard error) by island sides and soil depth using ggplot2 package in (Wickhm, 2016)**.** The principal component analysis (PCA) was performed on JMP (SAS Institute, Cary, NC).

3. Result and discussion

3.1. Erosion rate and bathymetry

The marsh edge erosion rate ranged from 71 cm yr^{-1} to 114 cm yr^{-1} with a mean value of 90.43 ± 4.4 cm yr^{-1} despite being relatively "protected" from waves by surrounding islands. However, the erosion rate on this island is half of that recorded at the islands facing directly into the open bay in Barataria Basin which have a mean erosion rate of 170.5 ± 17 cm yr^{-1} (Sapkota and White, 2019). The "protection" of this island by other islands reduces the fetch and act as barriers to the wind waves propagating from the open bay. The locally generated shallow water wind waves may be a dominant player in eroding otherwise "protected" marsh islands (Valentine and Mariotti, 2019).

The north and west side of the island experience significantly higher erosion (102.38 ± 5.2 cm yr^{-1}) rates ($p < 0.001$) than east and south side of the island (78.47 ± 3.3 cm yr^{-1}); though, the range of the erosion rates is constricted (71–114 cm yr^{-1}) (Table 2). The differences in erosion rates may be related to the speed, duration, and direction of the prevailing wind and fetch of the adjacent open water (Fagherazzi and Wiberg, 2009; Sapkota and White, 2019). The prevailing wind direction in the Barataria Basin is from the east, south, and west directions but with higher velocity from the north direction during winter frontal passage (Sapkota and White, 2019; Valentine and Marriotti, 2019). The greater intensity of the northerly wind may be the cause of the larger erosion rate on north side, whereas the greater duration of wind coupled with longer fetch is likely related to the greater erosion rate on west side of the island.

The estuarine depth relative to marsh surface at the edge of the marsh (+0.2 m) ranged from 35 to 45 cm whereas the depth at 16 m offshore ranged from 105 to 145 cm (Table 2). The edge erosion rate was weakly correlated (r = 0.24) with estuarine depth at the edge of the marsh but strongly correlated (r = 0.92) with depth at 16 m offshore suggesting a bathymetric impact on erosion. The deeper estuarine water produces waves with greater heights and helps in concentrating wave energy to the marsh; however, the shallow estuarine depth helps in wave dessipation. The wind waves not only erode the edge of the marsh but also scour the bottom of the estuary and increase estuarine depth (Fagherazzi and Wiberg, 2009; Mariotti et al., 2010). In addition to wave climate, the soil physiochemical properties and *in situ* degradation of SOM may affect the marsh edge erosion rate (Wang et al., 2017; Valentine and Mariotti, 2019; Sapkota and White, 2019).

3.2. Soil physiochemical properties

Soil bulk density and TC were significantly affected by depth and island side, but not by distance along the transects (Table 3). The bulk density of the marsh soil ranged from 0.17 ± 0.004 g cm^{-3} at the depth of 80–90 cm on the north side to 0.67 ± 0.21 g cm^{-3} at the depth of 40–50 cm on east side. The TC ranged from 26.15 ± 5.42 g kg^{-1} at the surface (0–10 cm) of south side to

Table 2
Mean marsh edge erosion rate, depth of estuary adjacent to marsh edge relative to marsh surface, and top 40 cm soil physiochemical properties on different sides of island. Figures in the parenthesis indicate standard error (n = 3).

Direction	Marsh edge erosion		Depth of estuary offshore		Top 40 cm soil	
	Measured days	Erosion rate (cm yr^{-1})	at +0.2 m (cm)	at +16 m (cm)	Bulk density (g cm^{-3})	Total carbon (g kg^{-1})
North	785	106.7 (5.42)	45	145	0.31 (0.01)	128.35 (3.21)
East	785	76.77 (5.60)	35	115	0.39 (0.02)	88.63 (9.87)
South	785	80.18 (4.54)	45	105	0.45 (0.02)	87.98 (4.64)
West	785	98.06 (9.43)	35	145	0.37 (0.03)	98.07 (4.92)

Table 3
p-values for fixed effects (depth, side, distance, and interactions) on soil physiochemical, porewater DOC, and porewater spectroscopic variables derived from ANOVA. The values in bold are significant (alpha value = 0.003).

Parameters	Depth	Side	Distance	Depth*side	Depth* Distance	Side* Distance	Depth*Distance*Side
BD	**<0.001**	**<0.001**	0.406	**<0.001**	**<0.001**	0.148	0.216
TC	**<0.001**	**<0.001**	0.542	**<0.001**	0.008	**<0.001**	0.48
DOC	**<0.001**	**<0.001**	0.091	**<0.001**	0.2526	0.159	0.279
$SUVA_{254}$	**<0.001**	**<0.001**	0.052	**<0.001**	0.092	0.029	0.296
$SUVA_{350}$	**<0.001**	**<0.001**	0.448	**<0.001**	0.171	0.113	0.576
S_{275}	0.509	0.004	0.703	0.989	0.638	0.757	0.442
FI	**<0.001**	**<0.001**	0.041	0.551	0.548	0.981	0.996
BIX	**0.002**	**<0.001**	0.04	0.828	0.953	0.681	0.999
HIX	**<0.001**	**<0.001**	0.159	**<0.001**	0.044	0.289	0.995

BD = Bulk density, TC = Total C, DOC = Dissolved organic C, SUVA = Specific UV absorbance.

287.47 ± 13.76 g kg^{-1} at the depth of 80–90 cm of north side. The bulk density and TC content of marsh (−2 m) and estuary cores (+0.2 and 16 m) were generally similar at corresponding depth for each distance. However, the surface of the estuarine bottom generally had lower TC content compared to the corresponding depth at the marsh and/or marsh edge, possibly related to the mineralization of SOM at the aerobic zone of soil water interface (Reddy and DeLaune, 2008). Overall, bulk density generally decreased with depth up to 150–160 cm and then increased, except for an increase at the depth of 40–50 cm related to a mud layer. Likewise, the TC generally increased with depth up to 150–160 cm and then markedly decreased, except for a decrease at 40–50 cm (Fig. 2a). The increase in TC with depth is consistent with studies conducted on the other parts of the Barataria Basin (Steinmuller and Chambers, 2019; Sapkota and White, 2021) but atypical for other coastal marsh sites (Webster and Benfield, 1986; Schipper and Reddy, 1995; Mendelssohn et al., 1999; Reddy and DeLaune, 2008). This increase in TC with depth may be related to the past depositional environment. These marshes were a continuous unfragmented fresh marsh with limited sediment supply (DeLaune, 1986). With accelerating sea-level rise and reduced river inflow, these marshes gradually became fragmented and transformed into intermediate to brackish marshes. As marsh fragmentation continues, there is a greater transport of C into the estuary. The higher bulk density and lower TC content at the depth of 40–50 cm have also been reported by studies on other Barataria Basin sites and may relate to past storm events or river channel switching (DeLaune et al., 2013; Steinmuller et al., 2020; Spera et al., 2020; Sapkota and White, 2021).

The depth of the estuary at the edge of the marsh relative to marsh surface was 35–45 cm (Table 2) and indicates that the initial depth of the erosion was approximately 35–45 cm. We have found that physiochemical properties of the top 40 cm soil are correlated with the erosion rates. The erosion rate was strongly negatively correlated (r = − 0.62) with bulk density whereas strongly positively correlated (r = 0.74) with TC content of top 40 cm deep soil and consistent with the literature (Table 2) (Sapkota and White, 2019). The soil with higher bulk density may require greater wind wave energy to erode compared to the soil with lower bulk density.

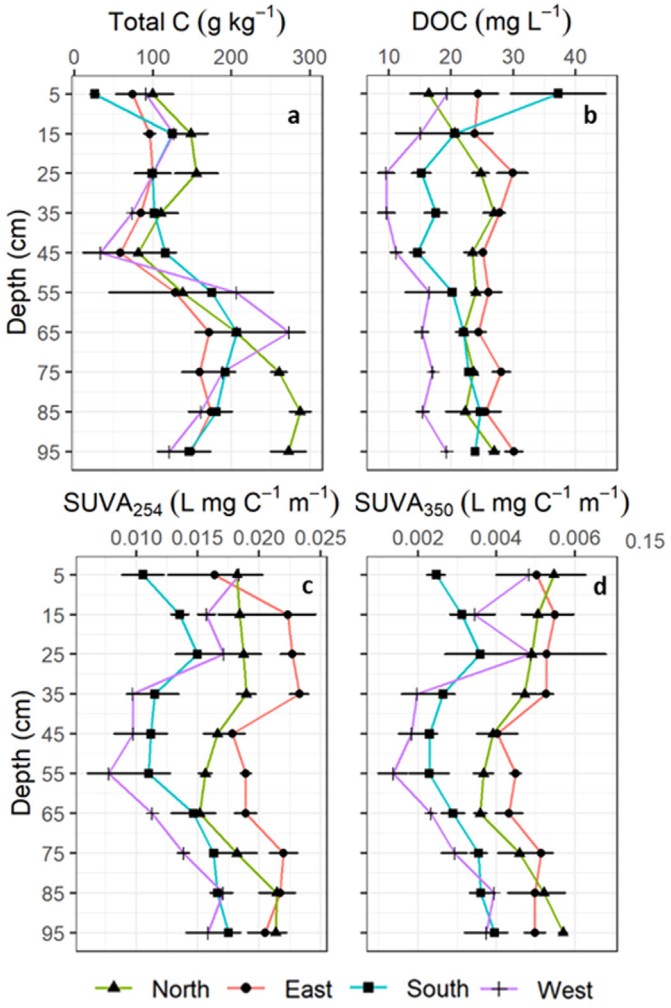

Fig. 2. The carbon speciation and complexity by sides and depth of intact marsh. a) Total soil carbon, b) porewater dissolved organic carbon (DOC), c) specific ultraviolet absorbance at 254 nm ($SUVA_{254}$) as a proxy for aromatic carbon, and d) specific ultraviolet absorbance at 350 nm ($SUVA_{350}$) as a proxy for lignin-like carbon.

3.3. Dissolved carbon concentrations

The water columns at the +0.2 m and +16 m distances were similar in DOC concentration on all sides of the island ($p > 0.05$) suggesting a well-mixed estuary. The mean DOC of estuarine water was 7.93 ± 0.05 mg C L^{-1}. The water column DOC concentration was lower than the porewater concentrations of surface soil (0–10 cm) for both the marsh and estuarine bottom.

The porewater DOC concentrations were significantly affected by the depth and island side (Table 3). The DOC ranged from 9.57 ± 1.3 mg C L^{-1} at a depth of 20–30 cm on west side to 37.23 ± 7.7 mg C L^{-1} at the surface (0–10 cm) of the south side. The DOC concentration on the south and west sides decreased up to 20–30 cm depth and then generally increased with depth (Fig. 2b). The DOC concentration at the north and east sides showed fluctuations, increasing slightly with depth. Overall, the north and east sides had greater DOC concentrations compared to south and west

sides. DOC concentration at the estuarine bottom (+0.2 m) was significantly smaller on north and east sides, significantly greater on south side, and similar in concentration on west side compared to the corresponding depth of the marsh soil (−2 m) indicating the complexity of the ongoing biogeochemical degradations. The DOC concentration was not correlated with the TC content of the soil indicating that flux and/or microbial activities are governing the decomposition process rather than the amount of the total soil carbon present. The erosion rate was negatively correlated ($r = -0.49$) with DOC concentration of top 40 cm soil porewater.

3.4. Porewater spectroscopic indicators

Porewater spectroscopic indicators provide a measure of biogeochemical degradation of DOC and serve as a proxy for the state of organic matter decomposition in the soil, Table 1, (Haywood et al., 2020; Steinmuller et al., 2020). The DOC normalized specific UV−visible absorbance ($SUVA_{254}$ and $SUVA_{350}$) significantly varied with depth and side (Table 3). Both $SUVA_{254}$ and $SUVA_{350}$ fluctuated but increased with depth on all sides (Fig. 2c and d) indicating higher aromatic carbon ($SUVA_{254}$) and lignin-like carbon ($SUVA_{350}$) content at depths (Weishaar et al., 2003; Zhang et al., 2020; Lei et al., 2020). This increase in aromatic and lignin-like DOC content with soil depth indicated the presence of more refractory carbon at depths. Likewise, the north and east sides of the island had significantly higher ($p < 0.001$) $SUVA_{254}$ and $SUVA_{350}$ than the south and west sides of the island indicating higher refractory carbon on the north and east sides. The SUVA ratio (the ratio of $SUVA_{350}$ to $SUVA_{254}$; $SUVA_{350}/SUVA_{254}$) (range = 0.14–0.34) decreased from 0.28 ± 0.01 at the surface to 0.21 ± 0.01 at 50–60 cm depth and then increased to 0.24 ± 0.01 at 90–100 cm at all sides. The highest SUVA ratio at the surface indicates the presence of more lignin-like carbon (~28%) possibly related to the quick degradation of the labile carbon at surficial soil (0–10 cm). The spectral slope (S_{275}) did not significantly vary across depth, side, or distance (mean = 0.8 ± 0.02 nm^{-1}) indicating the presence of lignin compounds with similar molecular weight throughout the soil depth (Chao et al., 2013; Fichot and Benner, 2012) (Table 3).

Spectroscopic indices including fluorescence index (FI), biological index (BIX), and humification index (HIX) provide information on the carbon parent material and degradation pathways (Haywood et al., 2018, 2020; Steinmuller et al., 2020). The FI, HIX, and BIX were significantly affected by depth and side (Table 3; Fig. 3). The FI values were <1.11 indicating the terrestrial source of the DOC present across the depth of the marsh and estuary soil (McKnight et al., 2001). The FI and BIX were significantly higher on south and west sides compared to north and east sides of the island indicating that the DOC on the south and west sides is less terrestrial and more microbial. The BIX values slightly decreased with depth, indicating the presence of microbial activities at all the depths studied. The slightly increasing trend of the HIX with depth indicates increasing refractory carbon content with depth and is well supported by the increasing trend of aromatic and lignin-like carbon (Song et al., 2019).

In addition, differences exist between surficial soil (0–10 cm) and below 10 cm in terms of carbon and spectroscopic indicators, at all sides and distance, indicate higher carbon degradation at the surface, while increased humification processes occur with increasing depth (Ibanez et al., 2003; Reddy and DeLaune, 2008; Rosa et al., 2005, Haywood et al., 2020). The lower concentration of the labile carbon at the surface is associated with higher microbial activities as indicated by the FI and BIX. The microbial activities, as indicated by the BIX, was present in significant amount across depth, and is consistent with the biogeochemical studies in Barataria Basin (Steinmuller et al., 2019; Steinmuller and Chambers, 2019; Haywood et al., 2020; Sapkota and White, 2021). Refractory carbon and humification increase with depth, as indicated by the terrestrial-like older material (FI and HIX), aromatic carbon ($SUVA_{254}$), and lignin-like carbon ($SUVA_{350}$) content.

A PCA was performed among the carbon and spectroscopic

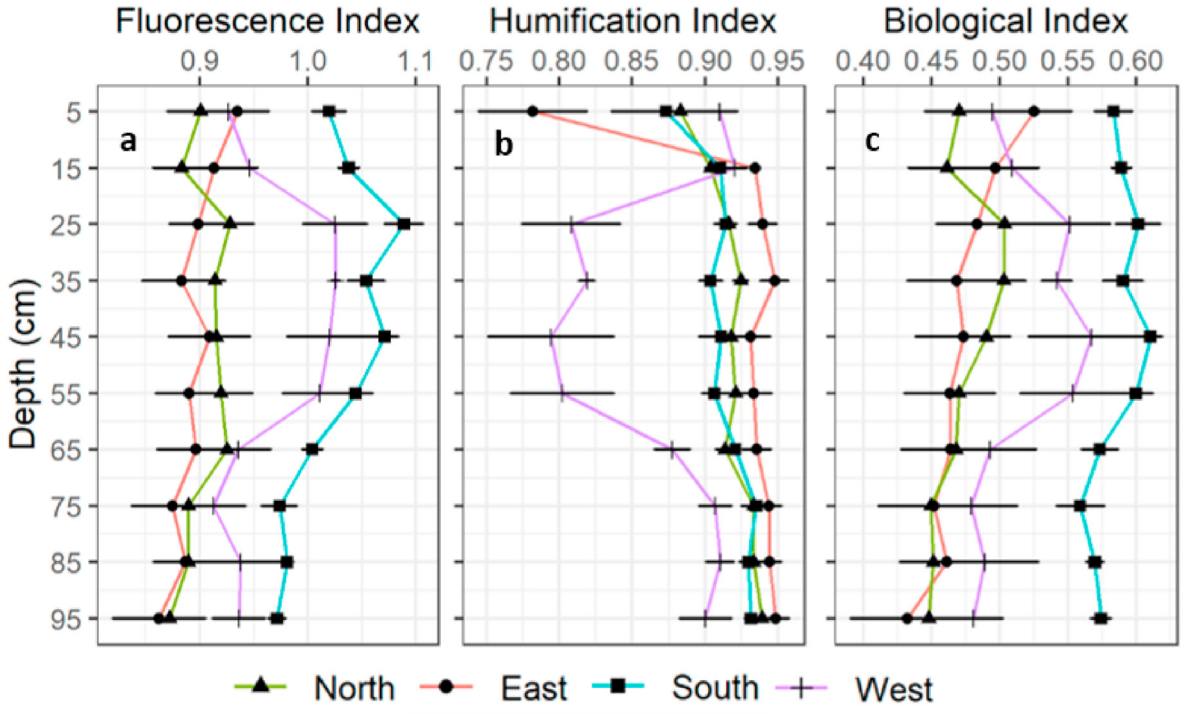

Fig. 3. The porewater spectroscopic indicators by sides and depth of intact marsh. (a) Fluorescence index (FI), (b) Humification index (HIX), and (c) Biological index (BIX).

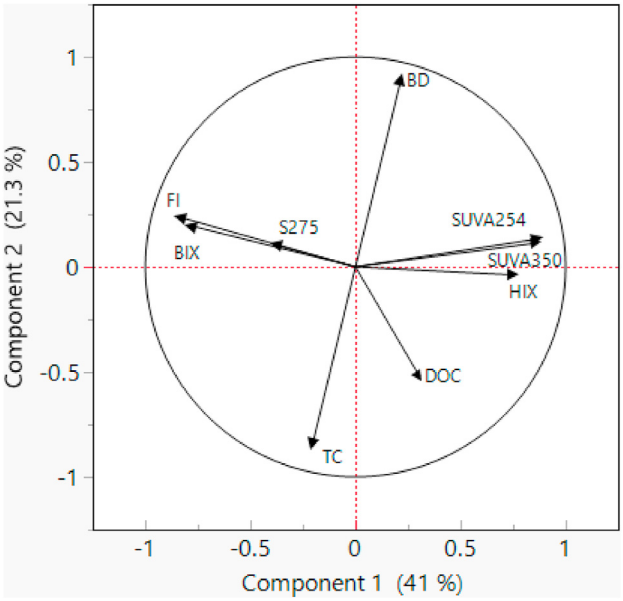

Fig. 4. Principal component analysis plot showing soil physiochemical properties, porewater DOC and spectroscopic variables into groups of humification (quadrant I) and biological variables (quadrant II).

variables (Fig. 4). Among the spectroscopic variables, the BIX and FI were grouped as biological variables whereas HIX, $SUVA_{254}$, and $SUVA_{350}$ were grouped as humification variables (Haywood et al., 2018; Haywood et al., 2020; Steinmuller et al., 2020). The variables within the carbon, biological, and humification groups were correlated with each other, supporting the results of different variables within each group. When the microbial communities are active, the BIX index is higher and degrades refractory carbon (terrestrial source) to labile carbon (aquatic source) leading to increased FI values. As the HIX increases, the carbon becomes more refractory and less energetically favorable for microbial communities degradation. The correlation between the spectroscopic variables is consistent with the studies conducted on the unprotected islands in the Barataria Basin (Haywood et al., 2020; Steinmuller et al., 2020).

3.5. Synthesis and implications

The north and west sides had greater erosion rates than east and south sides. However, the north and east sides had greater DOC and refractory carbon (aromatic and lignin-like) but less microbial activity and thus less organic matter degradation compared to south and west sides, indicating that carbon degradation did not alone correlate to edge erosion. This intersecting trend between erosion rate and porewater spectroscopic variables among four sides of the island indicates the complex nature of edge erosion drivers. The major factors responsible for edge erosion include wind speed, duration, and direction as well as fetch, tidal height, soil properties, and vegetation cover (Feagin et al., 2009; Sapkota and White, 2019; Valentine and Mariotti et al., 2019).

The edge erosion results in the export of the wetland soil carbon and nutrients into the adjacent estuary (Steinmuller et al., 2020). The wave scours and bottom shear stress continuously dislodges the submerged carbon from the estuarine bottom. Some studies in Barataria Basin have shown that the maximum depth of erosion is ~1.5 m and occurs between 50 and 150 m away from the edge of the marsh (Wilson and Allision, 2008; Sapkota and White, 2019). Unlike other sites, the north and west sides of the island attain ~1.5 m depth of erosion at a relatively short distance (16 m) offshore. The depth of the estuary bottom at 16 m offshore is greater at the east and south sides of this island compared to unprotected sites in the Barataria Basin (Sapkota and White, 2019). Overall, the rate of edge erosion in "protected" sites is relatively smaller but the depth of the estuary erosion is greater compared to unprotected sites. These "protected" islands are also highly vulnerable to losing large amounts of stored carbon and nutrients over a relatively short period. As soon as this "good quality" of the carbon, as indicated by the presence of labile carbon and microbial activities, erodes into the aerobic estuarine water, the mineralization generally increased by 4–6 times (Reddy and DeLaune, 2008; Steinmuller et al., 2019).

Horizontally, most of the carbon and spectroscopic variables were similar to the corresponding depth of the marsh soil except for the surface at the estuarine bottom. The SOM at the aerobic zone of the soil-water interface in the estuarine bottom undergoes rapid degradation compared to the depths, evidenced by the carbon and spectroscopic variables (Haywood et al., 2020). The similar value of variables between marsh and estuary cores indicates that there is no reburial of eroded marsh carbon but rather continued erosion and mineralization in estuaries, which is consistent with the findings of studies in the unprotected island and adjacent estuaries of Barataria Basin (Steinmuller et al., 2019; Steinmuller and Chambers, 2019; Vaccare et al., 2019; Haywood et al., 2020; Sapkota and White, 2021).

The results presented here indicate that marsh islands, relatively "protected" by the presence of surrounding islands, are also susceptible to losing large amounts of stored carbon in a relatively short period, converting the carbon pool of the erosional perimeters of these marshes to atmospheric CO_2. This means that edge erosion and the associated marsh fragmentation are occurring throughout the perimeter of marsh islands, including "protected" inner islands. This is a compounded effect as edge erosion not only releases centuries of stored carbon but also contributes to the loss of land area for any future atmospheric carbon sequestration (DeLaune and White, 2012; Sapkota and White, 2020). This is of concern as tidal salt marshes are one of the most productive ecosystems on Earth and are well recognized for their carbon sequestration and storage capabilities with minimal methane emission. Since, no single factor is responsible for marsh edge erosion, large restoration projects reconnecting river sediment to these marshes may help reduce this carbon loss from land to the atmosphere by reducing edge erosion rates (CPRA, 2017).

Our study was conducted in a coastal basin experiencing high relative sea-level rise (~12+ mm yr^{-1}) where the unprotected and relatively "protected" marsh islands are already experiencing a high rate of edge erosion. This finding indicates a pressing need for coastal restoration efforts to focus on slowing the erosion rates to prevent centuries of stored carbon from being released into the atmosphere (Sapkota and White, 2020). Other wetland-dominated coastlines across the globe that are projected to experience a comparable high relative sea-level rise in the coming decades will likely soon experience high erosion rates and CO_2 emission.

4. Conclusion

The *in situ* biogeochemical degradations of soil organic matter from the edge of eroding relatively "protected" marsh island and the adjacent estuarine bottom was studied using soil physiochemical properties, porewater DOM, and porewater spectroscopic indicators. The north and west sides of the island experiences a significantly greater edge erosion rate compared to east and south sides. However, the DOC and spectroscopic indicators show that the south and west sides of the island has greater *in situ* SOM degradation compared to north and east sides. It

is clear from this study that marsh edge erosion is a complex process mediated by several factors including soil physiochemical properties, organic matter degradation, and the factors regulating wave climate including wind energy and fetch. Future work should be focused on decreasing rates of erosion to slow the loss of this large C pool. This coastal basin experiences high relative sea-level rise at present and may serve as the proxy for the fate of the wetland-dominated coastlines projected to experience a high relative sea-level rise in the near future unless measures are taken to conserve the sequestered C. Increasing sea level also will continue to threaten the stability of Lousiana's coastal wetland C stocks which comprise 40% of all coastal wetlands in the contiguous United States.

Credit author statement

Michael P. Hayes: Conceptualization, Investigation, Methodology, Writing – original draft preparation; Yadav Sapkota: Conceptualization, Investigation, Methodology, Formal analysis, Writing – original draft preparation, Writing – review & editing; John R. White: Conceptualization, Investigation, Writing- Reviewing and editing, Supervision, Funding acquisition; Robert L. Cook: Writing-Reviewing and editing, Supervision, Funding acquisition.

Declaration of competing interest

The authors declare that they have no known competing financial interests or personal relationships that could have appeared to influence the work reported in this paper.

Acknowledgment

This work was supported by a collaborative National Science Foundation (NSF) Chemical Oceanography Grant # 1636052. M.P. Hayes was funded by a NSF Graduate Research Fellowship and Y. Sapkota was funded by an Economic Development Assistantship from Louisiana State University. Special thanks to Eddie Weeks for help with field work.

References

Bianchi, T.S., Cook, R.L., Perdue, E.M., Kolic, P.E., Green, N., Zhang, Y., Smith, R.W., Kolker, A.S., Ameen, A., King, G., 2011. Impacts of diverted freshwater on dissolved organic matter and microbial communities in Barataria Bay, Louisiana, USA. Mar. Environ. Res. 72 (5), 248–257.

Blum, M., Roberts, H., 2009. Drowning of the Mississippi Delta due to insufficient sediment supply and global sea-level rise. Nat. Geosci. 2, 488–491.

Breithaupt, J.L., Smoak, J.M., Bianchi, T.S., Vaughn, D.R., Sanders, C.J., Radabaugh, K.R., Osland, M.J., Feher, L.C., Lynch, J.C., Cahoon, D.R., Anderson, G.H., Whelan, K.R.T., Rosenheim, B.E., Moyer, R.P., Chambers, L.G., 2020. Increasing rates of carbon burial in southwest Florida coastal wetlands. J. Geophys. Res. Biogeosciences 125, 1–25. https://doi.org/10.1029/2019JG005349.

Bridgham, S., Megonigal, J., Keller, J., Bliss, N., Trettin, C., 2006. The carbon balance of North American wetlands *Wetlands*, 26, 889–916.

Chambers, L.G., Steinmuller, Havalend E., Breithaupt, J.L., 2019. Toward a mechanistic understanding of "peat collapse" and its potential contribution to coastal wetland loss. Ecology. https://doi.org/10.1002/ecy.2720.

Chao, X., Hossain, A., Jia, Y., 2013. Numerical Modeling of Flow and Sediment Transport in Lake Pontchartrain Due to Flood Release from Bonnet Carre Spillway. INTECH. Open Access Publisher.

Chmura, G., Anisfeld, S., Cahoon, D., Lynch, J., 2003. Global carbon sequestration in tidal, saline wetland soils. Global Biogeochem. Cycles 17 (12).

Choi, Y., Wang, Y., 2004. Dynamics of carbon sequestration in a coastal wetland using radiocarbon measurements. Global Biogeochem. Cycles 18.

Clark, C., Aiona, P., Keller, J., Bruyn, W.D., 2014. Optical characterization and distribution of chromophoric dissolved organic matter (CDOM) in soil porewater from a salt marsh ecosystem. Mar. Ecol. Prog. Ser. 516, 71–83.

Cook, R.L., Birdwell, J.E., Lattao, C., Lowry, M., 2009. A multi-method comparison of Atchafalaya Basin surface water organic matter samples. J. Environ. Qual. 38 (2), 702–711.

Couvillion, B., Beck, H., Schoolmaster, D., Fischer, M., 2017. Land area change in coastal Louisiana (1932 to 2016) scientific investigations Map 3381. U.S. Geol. Surv. Sci. Investig.

CPRA, 2017. Louisiana's Comprehensive Master Plan for a Sustainable Coast. *Coastal Protection and Restoration Authority (CPRA)*, Baton Rouge, LA.

DeLaune, R.D., 1986. The use of δ13C signature of C-3 and C-4 plants in determining past depositional environments in rapidly accreting marshes of the Mississippi River deltaic plain, Louisiana, USA. Chem. Geol. Isot. Geosci. 59 (C), 315–320. https://doi.org/10.1016/0168-9622(86)90080-1.

DeLaune, R., Kongchum, M., White, J., Jugsujinda, A., 2013. Freshwater Diversions as an ecosystem management tool for maintaining soil organic matter accretion in coastal marshes. Catena 107, 139–144.

DeLaune, R., Nyman, J., Patrick, W., 1994. Peat collapse, ponding, and wetland loss in a rapidly submerging coastal marsh. J. Coast Res. 1021–1030.

DeLaune, R., White, J., 2012. Will coastal wetlands continue to sequester carbon in response to an increase in global sea level?: a case study of the rapidly subsiding Mississippi river deltaic plain. Climatic Change 110 (1–2), 297–314.

Derrien, M., Lee, M.H., Choi, K., Lee, K.S., Hur, J., 2020. Tracking the evolution of particulate organic matter sources during summer storm events via end-member mixing analysis based on spectroscopic proxies. Chemosphere 252. https://doi.org/10.1016/j.chemosphere.2020.126445.

Fagherazzi, S., Wiberg, P.L., 2009. Importance of wind conditions, fetch, and water levels on wave-generated shear stresses in shallow intertidal basins. J. Geophys. Res.: Earth Surface 114 (3), 1–12. https://doi.org/10.1029/2008JF001139.

Feagin, R., Lozada-Bernard, S., Ravens, T., Moller, I., Yeager, K., Baird, A., 2009. Does vegetation prevent wave erosion of salt marsh edges? Proceedngs of the National Academty of Science of the United States of America 106, 10109–10113.

Fichot, G., Benner, R., 2012. The spectral slope coefficient of chromophoric dissolved organic matter (S275-295) as a traces of terrigenous dissolved organic carbon in river influenced ocean margins. Limnol. Oceanogr. 57, 1452–1466.

Georgiou, I.Y., FitzGerald, D.M., Stonei, G.W., 2005. The impact of physical processes along the Louisiana coast. J. Coast Res. 44, 72–89.

Haywood, B.J., White, J.R., Cook, R.L., 2018. Investigation of an early season river flood pulse: carbon cycling in a subtropical estuary. Sci. Total Environ. 635, 867–877.

Haywood, B., Hayes, M., White, J., Cook, R., 2020. Potential fate of wetland soil carbon in a deltaic coastal wetland subjected to high relative sea level rise. Sci. Total Environ. 1, 135185.

Huguet, A., Vacher, L., Relexans, S., Saubusse, S., Froidefond, J.-M., Parlanti, E., 2009. Properties of fluorescent dissolved organic matter in the Gironde Estuary. Org. Geochem. 40 (6), 706–719.

Ibanez, J., Hernandez-Esparza, M., Doria-Serrano, C., Fregoso-Infante, A., Singh, M., 2003. Environmental chemistry: fundamentals: snorthger science & business media, 2010: in tidal, saline wetland soils. Global Biogeochem. Cycles 17 (4).

Jankowski, K.L., Tornqvist, T.E., Fernandes, A.M., 2017. Vulnerability of Louisiana's coastal wetlands to present-day rates of relative sea-level rise. Nat. Commun. 8, 14792 https://doi.org/10.1038/ncomms14792.

Joshi, D.R., Clay, D.E., Clay, S.A., Smart, A.J., 2020. Seasonal losses of surface litter in northern great plains mixed-grass prairies. Rangel. Ecol. Manag. 73, 259–264. https://doi.org/10.1016/j.rama.2019.11.003.

Kirby, R., 2000. Practical implications of tidal flat shape. Continent. Shelf Res. 20, 1061–1077.

Kolic, P.E., Roy, E.D., White, J.R., Cook, R.L., 2014. Spectroscopic measurements of estuarine dissolved organic matter dynamics during a large-scale Mississippi River flood diversion. Sci. Total Environ. 485–486, 518–527.

Lei, L., Thompson, J.A., McDonald, L.M., 2020. Assessment of dissolved organic carbon and iron effects on water color between a forest and pasture-dominated fine-scale catchment in a Central Appalachian region, West Virginia. Environ. Sci. Pollut. Res. 27, 29464–29474. https://doi.org/10.1007/s11356-020-09251-9.

Leonardi, N., Ganju, N.K., Fagherazzi, S., 2016. A linear relationship between wave power and erosion determines salt-marsh resilience to violent storms and hurricanes. Proc. Natl. Acad. Sci. Unit. States Am. 113, 64–68. https://doi.org/10.1073/pnas.1510095112.

Li, C., White, J.R., Chen, C., Lin, H., Weeks, E., Galvan, K., Bargu, S., 2011. Summertime tidal flushing of Barataria Bay: transports of water and suspended sediments. J. Geophys. Res. 116 (C4).

Marani, M., D'Alpaos, A., Lanzoni, S., Santalucia, M., 2011. Understanding and predicting wave erosion of marsh edges. Geophys. Res. Lett. 38, 1–5. https://doi.org/10.1029/2011GL048995.

Mariotti, G., 2016. Revisiting salt marsh resilience to sea level rise: are ponds responsible for permanent land loss? Journal of Geophysical Restoration ResearchEarth Surface: Earth surface 1391–1407.

Mariotti, G., Fagherazzi, S., Wiberg, P.L., McGlathery, K.J., Carniello, L., Defina, A., 2010. Influence of storm surges and sea level on shallow tidal basin erosive processes. J. Geophys. Res.: Oceans 115 (11), 1–17. https://doi.org/10.1029/2009JC005892.

McKnight, D.M., Boyer, E.W., Westerhoff, P.K., Doran, P.T., Kulbe, T., Andersen, D.T., 2001. Spectrofluorometric characterization of dissolved organic matter for indication of precursor organic material and aromaticity. Limnol. Oceanogr. 46 (1), 38–48.

Mcleod, E., Chmura, G., Bouillon, S., Salm, R., Björk, M., Duarte, C., Lovelock, C., Schlesinger, W.H., Silliman, B.R., 2011. A bluenortht for blue carbon: toward an improved understanding of the role of vegetated coastal habitats in sequestering CO_2. Front. Ecol. Environ. 9 (10), 552–560.

McLoughlin, S., Wiberg, P., Safak, I., McGlathery, K., 2015. Rates and forcing of marsh edge erosion in a shallow coastal bay. Estuar. Coast 38, 620–638.

Mendelssohn, I.A., Sorrell, B.K., Brix, H., Schierup, H.H., Lorenzen, B., Maltby, E., 1999. Controls on soil cellulose decomposition along a salinity gradient in a Phragmites australis wetland in Denmark. Aquat. Bot. 64 (3–4), 381–398. https://doi.org/10.1016/S0304-3770(99)00065-0.

Morton, R., Bernier, J., Kelso, K., 2009. Recent subsidence and erosion at diverse wetland sites in the southeastern Mississippi delta plain. US Geological Series Open File Report.

Nyman, J.A., Carloss, M., Delaune, R.D., Patrick, H., 1994. Erosion rather than plant dieback as the mechanism of marsh loss in a n estuarine marsh. Earth Surf. Process. Landforms 19, 69–84.

Ohno, T., 2002. Fluorescence inner-filtering correction for determining the humification index of dissolved organic matter. Environ. Sci. Technol. 36 (4), 742–746.

Reddy, K.R., DeLaune, R.D., 2008. Biogeochemistry of Wetlands: Science and Applications. CRC press.

Rogers, K., Kelleway, J., Saintilan, N., Megonigal, J., Adams, J., Holmquist, J., Lu, M., Schile-Beers, L., Zawadzki, A., Mazumder, D., Woodroffe, C., 2019. Wetland carbon storage controlled by millennial-scale variation in relative sea-level rise. Nature 567, 91–95.

Rosa, A., Simoes, M., de Olierira, L., Rocha, J., Neto, L., Milori, D., 2005. Multimethod study of the degree of humification of humic substances extracted from different tropical soil profiles in Brazil's Amazonian region. Geoderma 127, 1–10.

Sapkota, Y., White, J., 2019. Marsh edge erosion and associated carbon dynamics in coastal Louisiana; A proxy for future wetland- dominated coastline world-wide. Estuar. Coast Shelf Sci. 226.

Sapkota, Y., White, J.R., 2020. Carbon offset market methodologies applicable for coastal wetland restoration and conservation in the United States: a review. Sci. Total Environ. 701, 134497 https://doi.org/10.1016/j.scitotenv.2019.134497.

Sapkota, Y., White, J.R., 2021. Long-term fate of rapidly eroding carbon stock soil profiles in coastal wetlands. Sci. Total Environ. 753, 141913 https://doi.org/10.1016/j.scitotenv.2020.141913.

Schipper, L.A., Reddy, R.R., 1995. In situ determination of detrital breakdown in wetland soil-floodwater profile. Soil Sci. Soc. Am. J. 1437, 565–568. https://doi.org/10.2136/sssaj1995.03615995005900020042x.

Schuerch, M., Spencer, T., Temmerman, S., Kirwan, M., Wolff, C., Lincke, D., McOwen, C., Pickering, M., Reef, R., Vafeidis, A., Hinkel, J., Nicholls, R., Brown, S., 2018. Future response of global coastal wetlands to sea-level rise. Nature 561, 231–234.

Song, F., Wu, F., Feng, W., Liu, S., He, J., Li, T., Zhang, J., Wu, A., Amarasiriwardena, D., Xing, B., Bai, Y., 2019. Depth-dependent variations of dissolved organic matter composition and humification in a plateau lake using fluorescence spectroscopy. Chemosphere 225, 507–516. https://doi.org/10.1016/j.chemosphere.2019.03.089.

Spera, A.C., White, J.R., Corstanje, R., 2020. Spatial and temporal changes to a hydrologically-reconnected coastal wetland: implications for restoration. Estuar. Coast Shelf Sci., 106728 https://doi.org/10.1016/j.ecss.2020.106728.

Steinmuller, H.E., Chambers, L.G., 2019. Characterization of coastal wetland soil organic matter: implications for wetland submergence. Sci. Total Environ. 677, 648–659. https://doi.org/10.1016/j.scitotenv.2019.04.405.

Steinmuller, H., Dittmer, K., White, J., Chambers, L., 2019. Understanding the fate of soil organic matter in submerging coastal welands soils: a microcosm approach. Geoderma 337, 1267–1277.

Steinmuller, H., Hayes, M., Hurst, N., Sapkota, Y., Cook, R., White, J., Chambers, L., 2020. Does edge erosion alter coastal wetland soil properties? A multi-method biogeochemical study. Catena 187, 104373.

Traversa, A., D'Orazio, V., Mezzapesa, G.N., Bonifacio, E., Farrag, K., Senesi, N., Brunetti, G., 2014. Chemical and spectroscopic characteristics of humic acids and dissolved organic matter along two Alfisol profiles. Chemosphere 111, 184–194. https://doi.org/10.1016/j.chemosphere.2014.03.063.

Vaccare, J., Meselhe, E., White, J., 2019. The denitrification potential of eroding wetlands in Barataria Bay, LA, USA: implications for river reconnection. Sci. Total Environ. 686, 529–537.

Valentine, K., Mariotti, G., 2019. Wind-driven water level fluctuation drives marsh edge erosion variability in microtidal coastal bays. Continent. Shelf Res. 176, 76–89.

Wang, H., Van der Wal, D., Li, X., Van Belzen, J., Herman, P., Hu, Z., Ge, Z., Zhang, L., Bouma, T., 2017. Zooming in and out: scale dependence of sxrinsic and intrinsic factors affecting salt marsh erosion. Journal of Geophysical Research:toration Earth Surface 122, 1455–1470.

Wang, Y., Zhang, D., Shen, Z., Feng, C., Chen, J., 2013. Revealing sources and distribution changes of dissolved organic matter (DOM) in pore water of sediment from the Yangtze estuary. PloS One 8, e76633.

Watanabe, A., Moroi, K., Sato, H., Tsutsuki, K., Maie, N., Melling, L., Jaffé, R., 2012. Contributions of humic substances to the dissolved organic carbon pool in wetlands from different climates. Chemosphere 88, 1265–1268. https://doi.org/10.1016/j.chemosphere.2012.04.005.

Webster, J.R., Benfield, E., 1986. Vascular plant breakdown in freshwater ecosystems. Annu. Rev. Ecol. Systemat. 17, 67–94.

Weishaar, J.L., Aiken, G.R., Bergamaschi, B.A., Fram, M.S., Fujii, R., Mopper, K., 2003. Evaluation of specific ultraviolet absorbance as an indicator of the chemical composition and reactivity of dissolved organic carbon. Environ. Sci. Technol. 37, 4702–4708. https://doi.org/10.1021/es030360x.

White, E., Messina, F., Moss, L., Meselhe, E., 2018. Salinity and marine mammal dynamics in barataria basin: historic patterns and modeled diversion scenarios. Water 10, 1015.

Whiting, G., Chanton, J., 2001. Greenhouse carbon balance of wetlands: methane emission versus carbon sequestration. Tellus 53, 521–528.

Wickham, H., 2016. ggplot2: Elegant Graphics for Data Analysis. Springer-Verlag, New York.

Williams, H., Flanagan, W., 2009. Contribution of Hurricane Rita Storm surge deposition to long-term sedimentation in Louisiana coastal woodlands and marshes. Journal of Coastal Restoration 56, 1671–1675.

Wilson, C.A., Allison, M.A., 2008. An equilibrium profile model for retreating marsh shorelines in southeast Louisiana. *Estuarine*. Coastal and Shelf Science 80 (4), 483–494.

Wolters, M., Bakker, J., Bertness, M., Jefferies, R., Moller, I., 2005. Saltmarsh erosion and restoration in south-east England; Squeezing the evidence requires realignment. J. Appl. Ecol. 42, 844–851.

Zhang, Z., Teng, C., Zhou, K., Peng, C., Chen, W., 2020. Degradation characteristics of dissolved organic matter in nanofiltration concentrated landfill leachate during electrocatalytic oxidation. Chemosphere 255, 1–9. https://doi.org/10.1016/j.chemosphere.2020.127055.